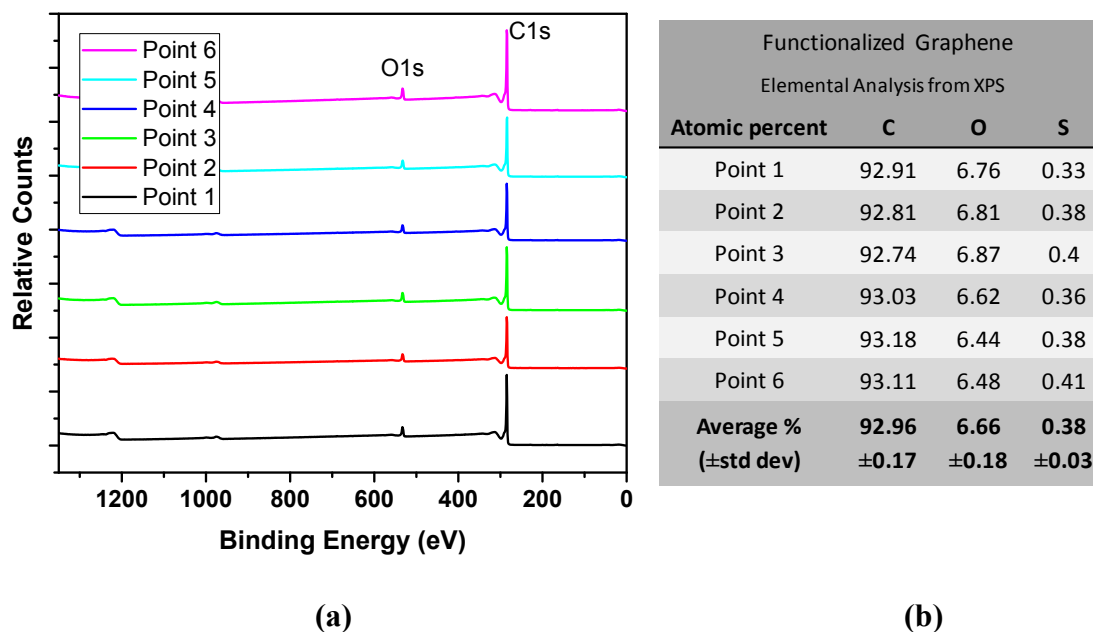


## **Supporting Information Section**

### **Graphene Characterization**

#### ***1. X-ray photoelectron spectroscopy analysis of the graphene***

X-ray photoelectron spectroscopy (XPS) (K-Alpha, Thermo Scientific) was used to analyze graphene batches from the oxygen functionalization procedures. Specifically, a powder graphene sample was put on double-sided tape on a glass substrate, then XPS characterized its elemental composition. A monochromated Al K $\alpha$  ( $h\nu = 1436.6$  eV) x-ray source (36W, 400  $\mu\text{m}$  diameter spot) was used to collect the resulting data. Survey scans (0-1350 eV) were done for each sample, with the pass energy (CAE) at 200 eV and step size at 1 eV. Narrow scans (C1s: 280-298 eV, O1s: 525-545eV) were done at pass energy (CAE) of 50 eV and step size of 0.1 eV. Both survey scan and narrow scan spectra were shifted to the main peak of carbon at 284.8eV. The relative abundance of elements was found via Avantage software (Thermo Scientific), which integrated and compared the area under the carbon (C1s), oxygen (O1s), and sulfur (S2p) photoemission peaks. Presented below are spectral comparisons from 6 different spots of an oxygen functionalized graphene sample.



**Figure S1.** (a) XPS survey spectra of graphene samples showing photoemissions from oxygen (O1s), nitrogen (N1s), carbon (C1s), and sulfur (S2p). (b) Elemental analysis summary from XPS data of oxygen, nitrogen, carbon, and sulfur expressed in atomic %.

From the XPS survey scans in Figure S1a, it is evident that the 6 points exhibit carbon-1s and oxygen-1s photoelectron emissions at  $\sim 285\text{eV}$  and  $\sim 533\text{eV}$ , respectively. Although less evident, there was also a photoemission from S2p at  $\sim 166\text{eV}$ . The atomic percent for each spot, based on peak area found by the Advantage system, and the average are summarized in Figure S1b. Carbon, oxygen, and sulfur content of the functionalized graphene is approximately 92.96%, 6.66%, and 0.38%, respectively.

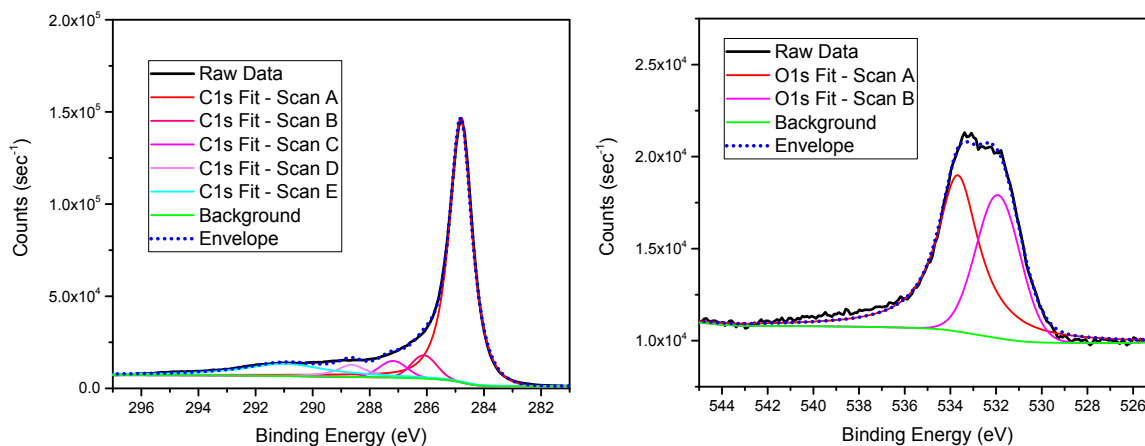


**Figure S2.** XPS narrow scan (C1s-top and O1s-bottom) spectra of functionalized graphene sample. The fitted peaks within the narrow scan spectra provide support for the bonding environments of the elements.

Narrow scan XPS spectra for a representative spot from the graphene sample are shown in Figure S2, shedding light on the chemical state (atomic environment) of the carbon and oxygen atoms within the graphene matrix. Since the graphene has been functionalized by oxygen, photoemission events from carbon (C1s) are expected to shift to higher binding energies that correspond to hydroxyl, carbonyl, and carboxylic acid functionalities—centered around 286.0, 287.0, and 288.5 eV, respectively. The peak at ca. 284.8eV is from the main carbon backbone of aliphatic/aromatic ( $sp^3/sp^2$ ) carbons, while the broad peak at ca. 291.0eV is a result of the shake-up caused by the many bonds in the system. By using peak fitting analysis in the Avantage software, it is possible to fit multiple curves to the raw data (black line in Figure S2) and compare this to the "envelope"(blue dotted line in Figure S2), which is a combination of the fitted curves. These individual curve fits provide estimates of the peak positions; additionally, relative contributions from each of these atomic environments are able to be estimated by integrating the area under the curve and above the baseline (green line in Figure S2). It was

determined that the most prominent peak occurs for the aromatic and aliphatic carbons around  $284.81 \pm 0.02 \text{ eV}$  with a contribution of  $77.61 \pm 1.68\%$ . The carbon environments for  $\underline{\text{C}}\text{-OH}$ ,  $\underline{\text{C}}=\text{O}$ , and  $\underline{\text{C}}\text{OOH}$  were centered around  $286.11 \pm 0.06 \text{ eV}$ ,  $287.16 \pm 0.06 \text{ eV}$ , and  $288.58 \pm 0.06 \text{ eV}$ , respectively; percent contributions based on area under the fitted curves for each of these environments were  $5.62 \pm 0.63\%$ ,  $4.56 \pm 0.24\%$ , and  $4.18 \pm 0.93\%$ , respectively. No contribution was determined for the broad fitted peak at  $\sim 291 \text{ eV}$  since this is a satellite peak due to \* interactions, and not the various functional groups. The corresponding narrow scan photoemission spectra for oxygen (O1s) show the contribution from oxygen bond singly and doubly to carbon:  $533.61 \pm 0.06 \text{ eV}$  due to  $\text{C}-\underline{\text{O}}$  ( $62.10 \pm 2.47\%$  contribution) and  $531.86 \pm 0.06 \text{ eV}$  due to  $\text{C}=\underline{\text{O}}$  ( $37.90 \pm 2.47\%$  contribution). XPS references for C1s and O1s peak fit positions (Fig. S2) were assigned according to the literature<sup>1,2</sup>.

## ***2. Infrared spectroscopy***

Infrared spectroscopy (Thermo Scientific FTIR Nicolet Model 6700 Spectrometer) was used to analyze the powder samples that were combined with KBr and pressed into pellets. The transmission E.S.P method was utilized, with 32 scans for both the background and sample being completed in the  $4000$  to  $400 \text{ cm}^{-1}$  spectral region. Other relevant instrument parameters are as follows: resolution =  $4.0$ , Sample gain =  $1.0$ , optical velocity =  $0.6329$ , and aperture =  $8.00$ . Figure S3 displays the resulting FTIR spectra for a sample of functionalized graphene. Peaks due to hydroxyl groups are present at  $3444 \text{ cm}^{-1}$  (O–H stretch) and  $1394 \text{ cm}^{-1}$  (C–O–H in plane bend). Multiple peaks are present due to C–H bonds, of which bands at  $2921 \text{ cm}^{-1}$  and  $2850 \text{ cm}^{-1}$  are due to stretching of CH and CH<sub>2</sub> groups, respectively, and a band at  $1464 \text{ cm}^{-1}$  is characteristic of C–H bending. Carbon-oxygen groups exhibit vibrations at  $1711 \text{ cm}^{-1}$  due to C=O stretch and at  $1182 \text{ cm}^{-1}$  due the C–OH stretch. The large sp<sup>2</sup> carbon lattice presents

aromatic stretching vibration bands at  $1641\text{ cm}^{-1}$  and  $1572\text{ cm}^{-1}$ . These peaks were assigned according to the literature.<sup>3,4</sup>

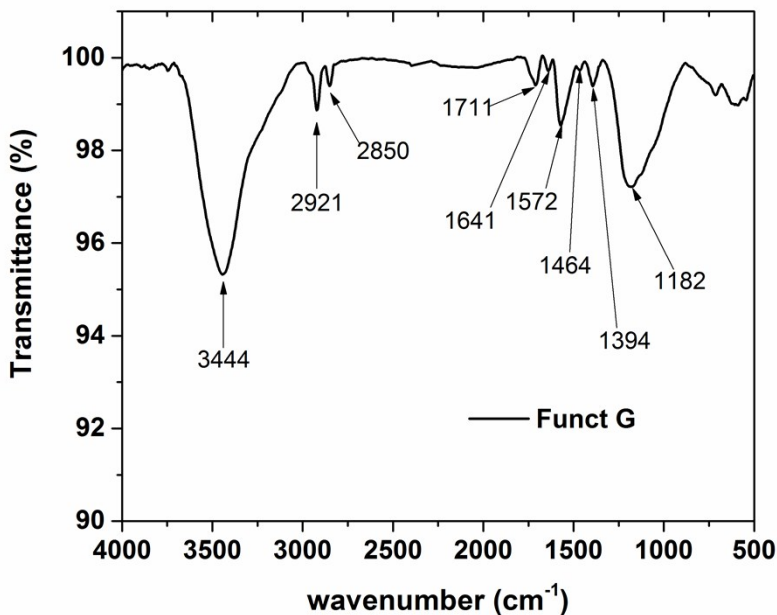


**Figure S3.** FTIR spectrum of functionalized graphene sample; wavenumbers for prominent bands are noted.

### ***3. Graphene size and thickness analysis (geometric analysis)***

#### ***(a) Atomic force microscopy (AFM)***

Slightly oxidized graphene solution was prepared in  $0.5\text{ }\mu\text{g/ml}$  concentration in DI water and sonicated for 6 hours. The final solution was centrifuged at 3200 rpm, then around  $5\text{ }\mu\text{L}$  of the supernatant was placed on silicon wafer and left to dry under vacuum. Dried flakes were imaged under AFM, figure S4 A. In order to analyze the flake size and thickness distribution, around 1400 flakes were imaged and histograms were plotted. Average height of graphene flakes was

estimated from graphene thickness was around 1.5-3 nm (Figure S4 C), and the average of flake size was around 100 nm (Figure S4 B).

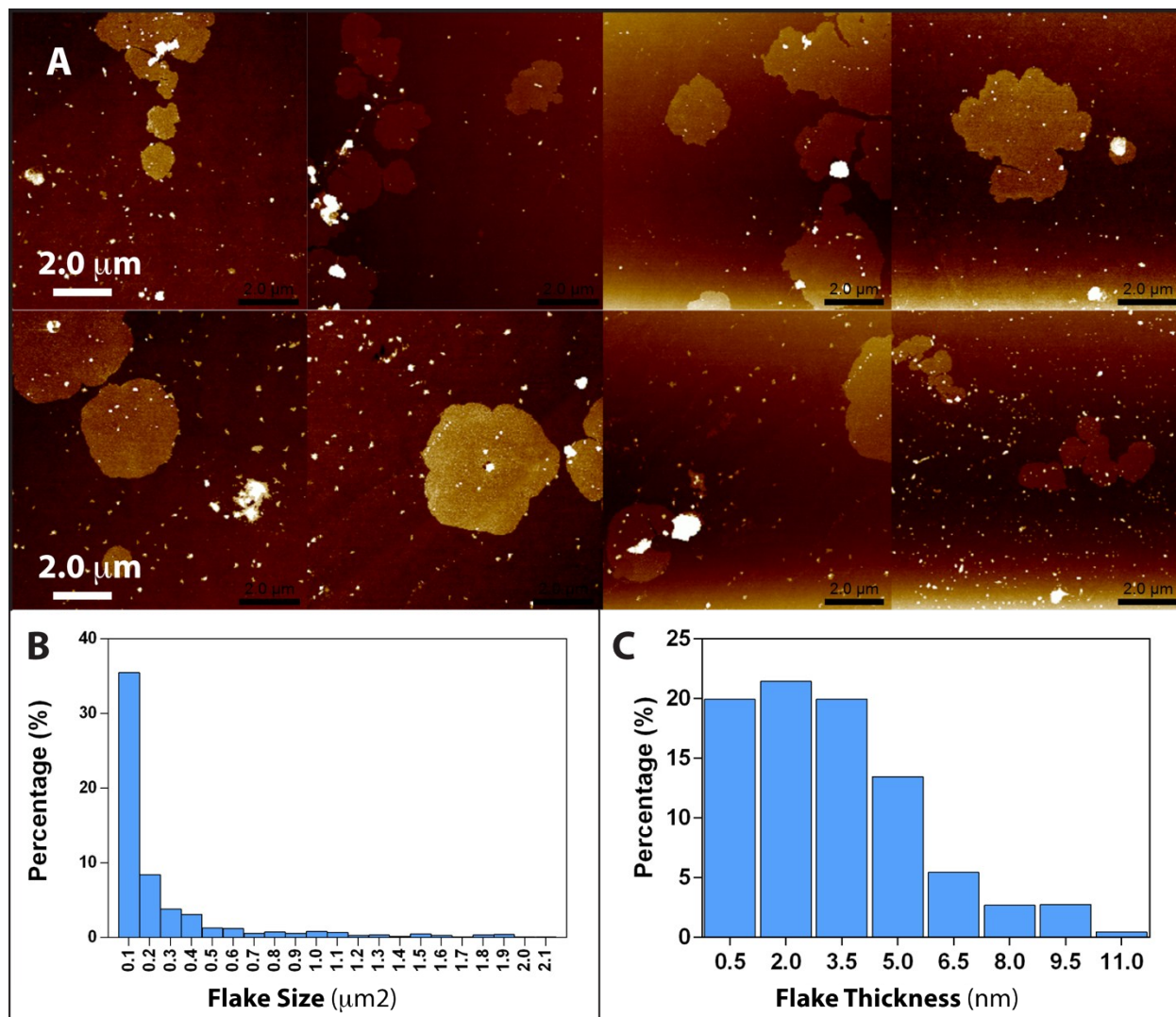


**Figure S4.** AFM images of low oxidized graphene (LOG) flakes distributed over silicon wafer. A) eight AFM images of graphene flaks, B) flake size distribution histogram showing that most of the flakes have area around 100-200 nm<sup>2</sup>, C) flake thickness histogram showing that most of the flakes have thickness around 0.5-3.5 nm.

*(b) Transmission electron microscopy (TEM)*

Slightly oxidized graphene solution was prepared in 0.5 $\mu\text{g/ml}$  concentration in DI water and sonicated for 6 hours. The final solution was centrifuged at 3200 rpm, then around 5 $\mu\text{L}$  of the supernatant was placed on TEM grid and left to dry under vacuum. Dried flakes were imaged under TEM (80kV).

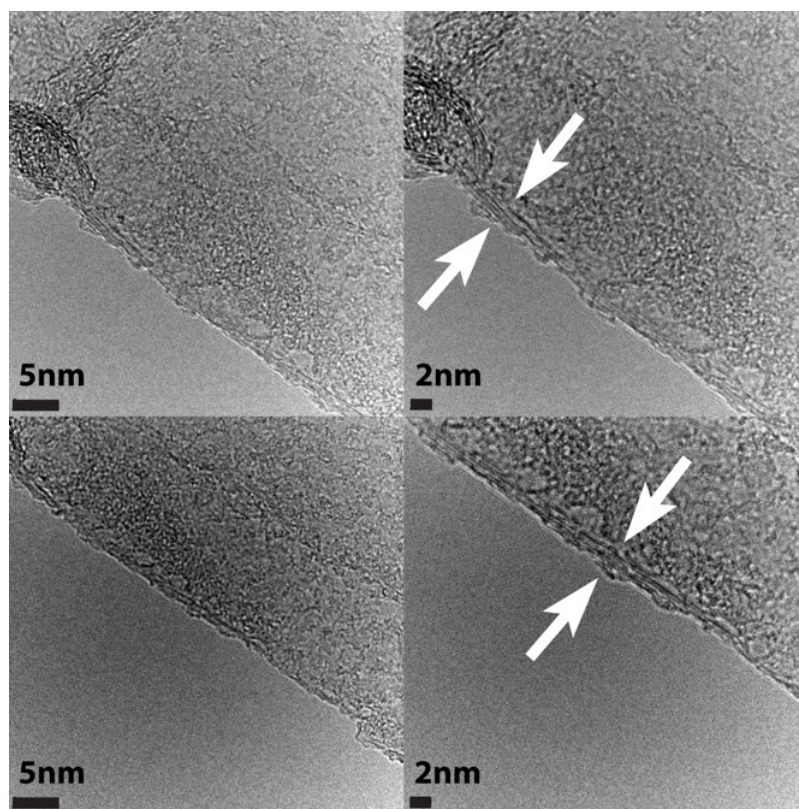


**Figure S5.** HRTEM Images of LOG flakes distributed over grid. Images were taken with 80kV.

## Evidence of graphene association (internal/surface)

### 1. Photoacoustic microscopy (PAM)

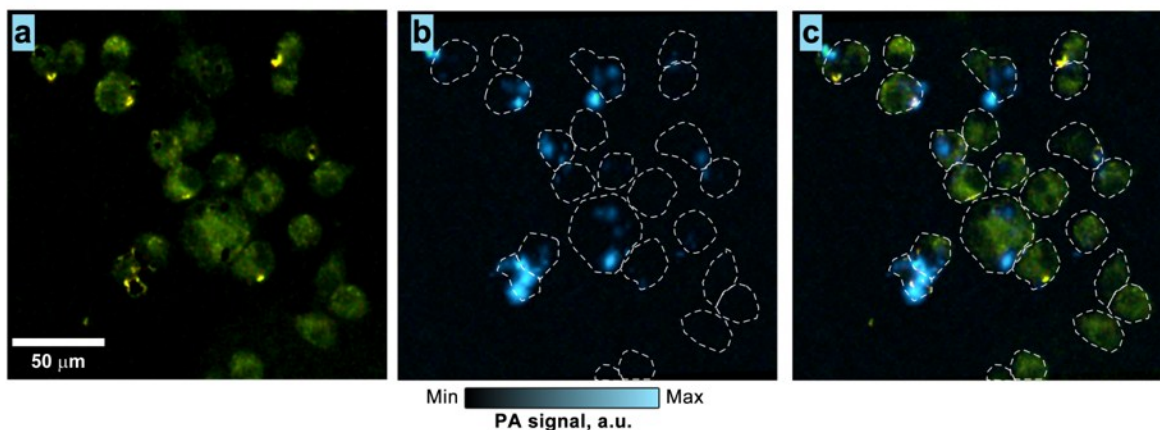


**Figure S6.** PA quantification of graphene association of graphene found with JAWSII cells: a) side illumination imaging of cells (light scattering contrast) used to manually identify individual cell outlines (white dash); b) PA imaging data merged with cell outline data (white dash) showing that most graphene is located within cell borders; c) merged images. Laser parameters: 532 nm, 10 kHz, laser fluence of 45 mJ/cm<sup>2</sup>.

#### *(a) Signal processing in PA detection*

In PA detection, the absorption of excitation laser light is causing fast expansion of the sample and generation of ultrasound waves that are recorded by a water-coupled transducer. Amplitudes of ultrasound waves (or an amplitude of a PA signal recorded by a transducer) from a point-like target is directly proportional to laser fluence and light absorption of this target (Figure S7). Here, each pixel of a PA image was calculated as an amplitude of PA signal (difference between maximal and minimal transducer voltage for a recorded signal) from a point-like source illuminated by a focused laser beam (lateral resolution of 2.3 μm). A layer of adhered cells is

thin (5-10  $\mu\text{m}$ ) compared to the axial resolution of the 20 MHz transducer (80  $\mu\text{m}$ ). No additional data processing (i.e. Hilbert's transform of the PA signal) was performed. Thus, for each position of the laser scanner (coded with XY coordinates) we acquired one value of PA signal amplitude. This data was used to build color-coded 2D PA images (**Figure S7**).

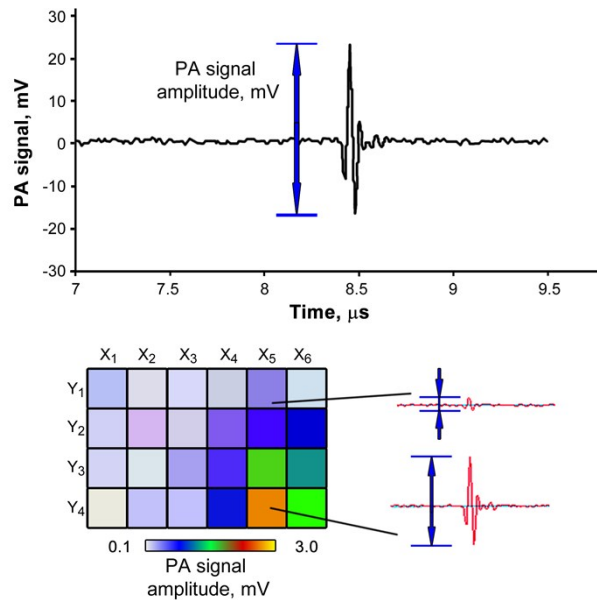


**Figure S7.** Principles of PA signal calculation for a typical PA signal trace acquired from the sample. The corresponding PA signal amplitude is calculated as a difference between maximal and minimal transducer voltage for the selected trace. Scheme below shows how PA signal amplitudes and XY laser beam position (laser scanner coordinates) were used to construct 2D PA images.

Since PA signal amplitude cannot be negative we have corrected all the measurements in order to account for electronic noise of the detection system. The background signal in PA experiments is mostly electronic and thermal noise in the detection system. Using control samples (no

graphene) we have calculated mean amplitude of electronic noise for PA signals. Next, for the samples of cells with graphene we calculated corrected signal as  $PA_c = PA_{\text{recorded}} - PA_{\text{noise}}$  for each pixel. Summation of corrected PA signals for a region of interest corresponding to a cell was used to quantify total graphene uptake by this cell.

***(b) The sensitivity of PA quantification technique***

The presented here technique for quantification of graphene-based nanomaterials (GBNs) among single cells was optimized for the selected JAWSII cell lines featuring high uptake of the nanoparticles with the range of graphene concentrations in 1-40 pg/cell. The PAM calibration data was acquired using uniform graphene films (Figure 3e). For each film, we visualized multiple locations throughout each sample and calculated PA signal as a function of the sample area, Figure S8. Given QCM data on the density of graphene film ( $\text{pg}/\mu\text{m}^2$ ) we calculated PA signal integrated over film area as a function of the film mass. The limit of detection was calculated from the calibration graph data and PA signal for control samples (triple standard deviation of the control signal). In the current configuration, the LOD was estimated as 200 fg of graphene. However, further improvements in detection sensitivity are possible. First, averaging of multiple PA signals, Figure S8, reduces detection noise as  $\sqrt{N}$ , where N is the number of averaged pulses. In this case imaging time is increased proportionally. Second, the energy of the excitation laser can be increased to induce higher pressure at the graphene flake, Figure S8. This increases the pressure of the ultrasound waves reaching the detection system. The use of higher energy pulses is disadvantageous due to possible sample damage that is most profound in thick graphene films used as calibration samples. In this work laser energy of 1.9 nJ/ pulse ( $45 \text{ mJ}/\text{cm}^2$  over  $2.3 \mu\text{m}$  sized laser spot) was selected as an optimal balance between sensitivity and laser

damage to thick films of graphene on glass. Higher amounts of deposited thermal and acoustic energy disrupted and damaged thin graphene films on a glass substrate. In cells the damage is less obvious due to flexible cell structure and non-homogeneous material distribution. An increase in laser energy up to 5-6 nJ/pulse did not cause any major disturbances during PA imaging of graphene flakes within cells, however, damage to calibration films was obvious. Hence, the ideal approach toward further reducing limits of detection for PAM is in combination of higher signal averaging with careful increasing laser fluence on the sample. Further work is needed to prove PAM accuracy at sub-pg graphene mass levels using other techniques to characterize graphene films on glass. A combination of AFM and PAM may allow characterization of single flakes and PA quantification at the same time. Unfortunately, efficient combination of AFM and PAM is complicated since PAM requires water medium for acoustic coupling.

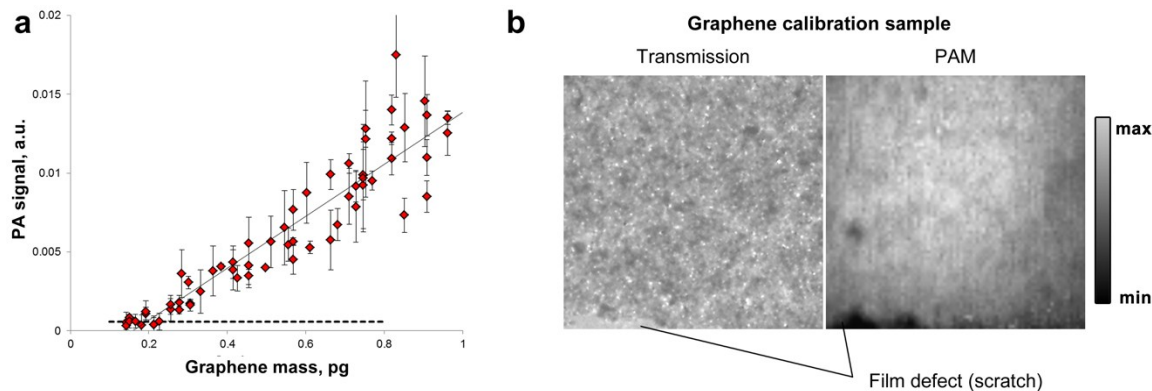


**Figure S8.** PAM calibration using graphene films: a) PAM calibration for low graphene mass (up to 1 pg, zoomed-in portion of Fig. 3e). Each dot corresponds to integrated PA signal over a certain area on the sample surface. Error bars were calculated by acquiring PA signal for the same area size, but from different parts of the same sample. Dash line shows a triple electronic

noise standard deviation level. b) Typical PAM and transmission images of a calibration graphene film.

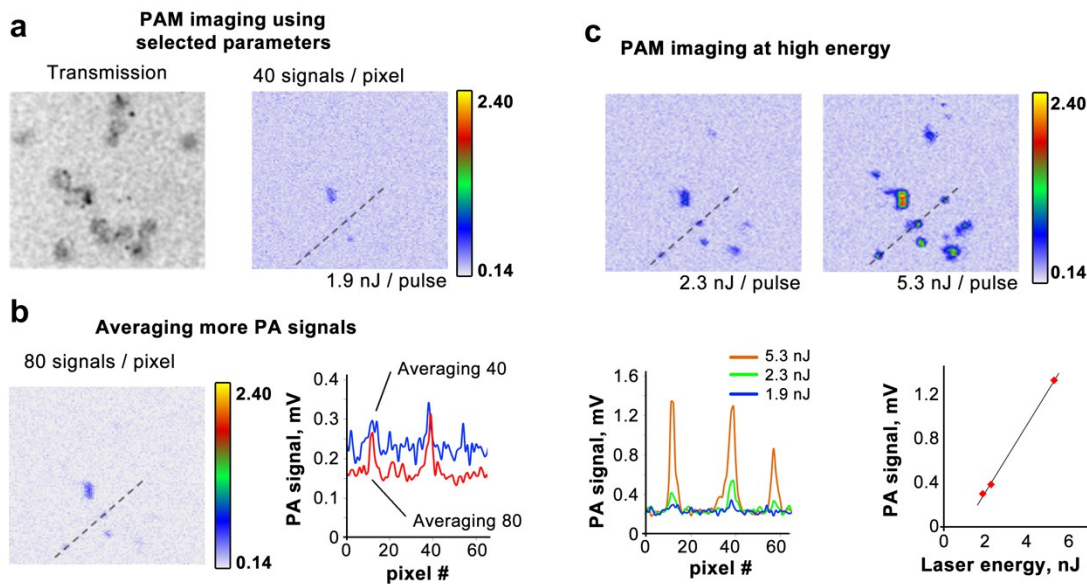


**Figure S9.** Possible avenues toward improving detection sensitivity in PAM. a) PA detection of graphene in JAWSII cells incubated with  $1\mu\text{g}/\text{mL}$  of the NPs for 4h. Detection parameters are identical to those used throughout this study; b) PA image of the same sample acquired using high number of averaged PA signals per pixel (80 signals/pixel). Graph shows PA signal along the dash line and a decrease in the level of noise; c) PA image of the sample at higher laser energy revealing more graphene particles. Graphs (bottom) show PA signal along dash line (left) and PA signal for one of the clusters as a function of laser energy (right).

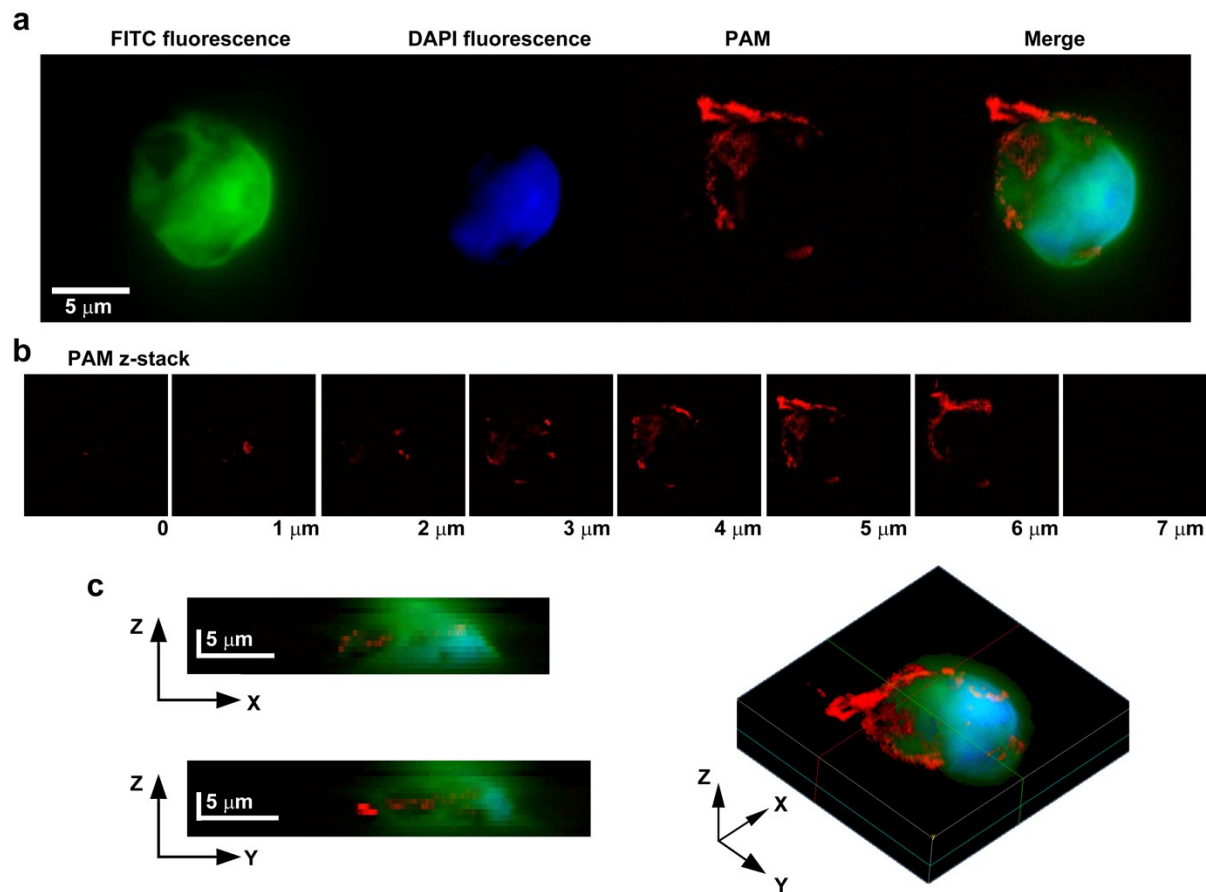


**Figure S10.** Internalization of graphene by JAWSII cells visualization by high resolution PA and fluorescence microscopy: a) individual fluorescence and PAM images of a single JAWSII cell incubated with 1 μg/mL of graphene for 4h; b) full z-stack of PAM images for the cell; c) 3D reconstruction of cell absorption by ImageJ.

**Video S1.** Bright-field microscopy and high-resolution PA mapping of graphene internalization by JAWSII cells. A stack containing a total of 12 PA and transmission images was acquired with 1 μm axial displacement steps.

**Video S2.** High-resolution fluorescence and PA mapping of graphene internalization by JAWSII cells. A stack containing a total of 14 PA and fluorescence (FITC and DAPI stains) images was acquired with 1  $\mu\text{m}$  axial displacement steps.

### ***2. TEM imaging of the JAWSII cells before and after exposure to graphene***

TEM images of both the control and the graphene exposed JAWSII were obtained by JEOL JEM-2100F (JEOL USA) at 80kV.

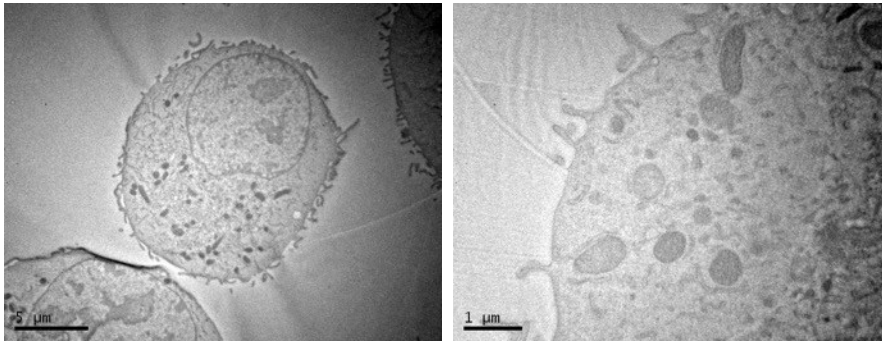


**Figure S11.** TEM images for JAWSII cells without graphene treatment (control). TEM images were obtained by JEOL JEM-2100F (JEOL USA) at 80kV.

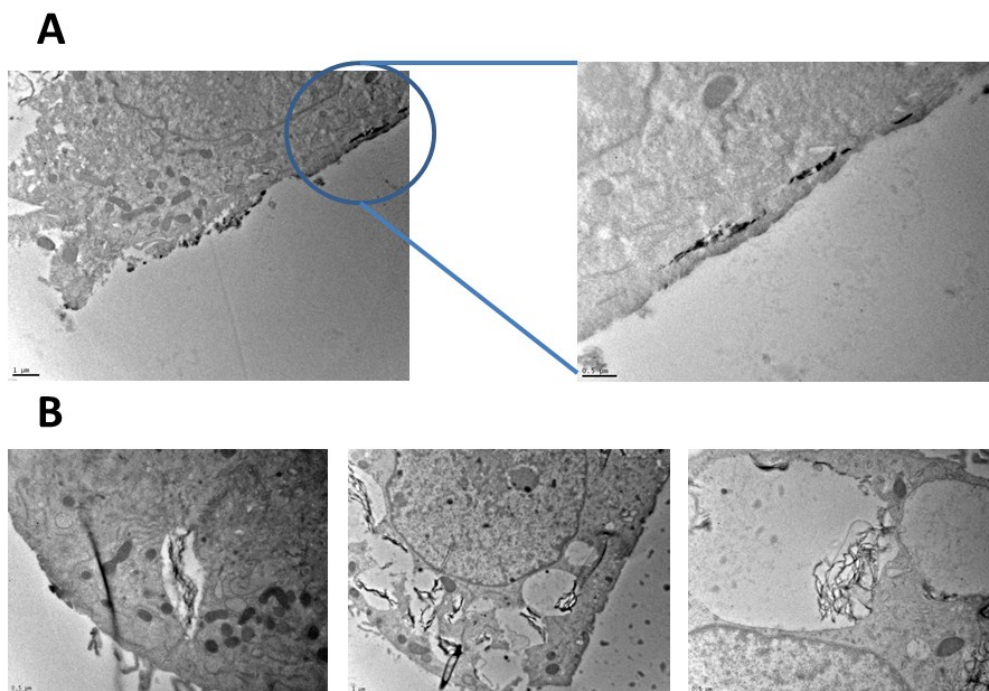


**Figure S12.** TEM images for JAWSII cells incubated with  $1\mu\text{g/ml}$  graphene for 24 hours. TEM images of both the control and the graphene-exposed JAWSII were obtained by JEOL JEM-2100F (JEOL USA) at 80kV.

### ***3. Raman z-scan mapping***

In order to estimate that the collected signal of graphene (D-Band) whether it was from the surface or from the cytoplasm, Raman mapping was conducted on JAWSII cells that incubated with  $50\mu\text{g/ml}$  for 6h as a representative example. Mapping procedure was performed as 3D (x,y,z) scan: x-y plain (JWASII) was chosen to cover the whole cell, then z plain was covered from -20 to 20  $\mu\text{m}$ , with 2 $\mu\text{m}$  increment. The results were plotted in the following figures S13(a-b), and supporting video (Video S3). Clearly, when compare Raman mapping images with the optical image of JWASII cell (BF insertion S13a), we conclude that the signal is coming from the attached graphene flakes on the membrane and from inside the cell.

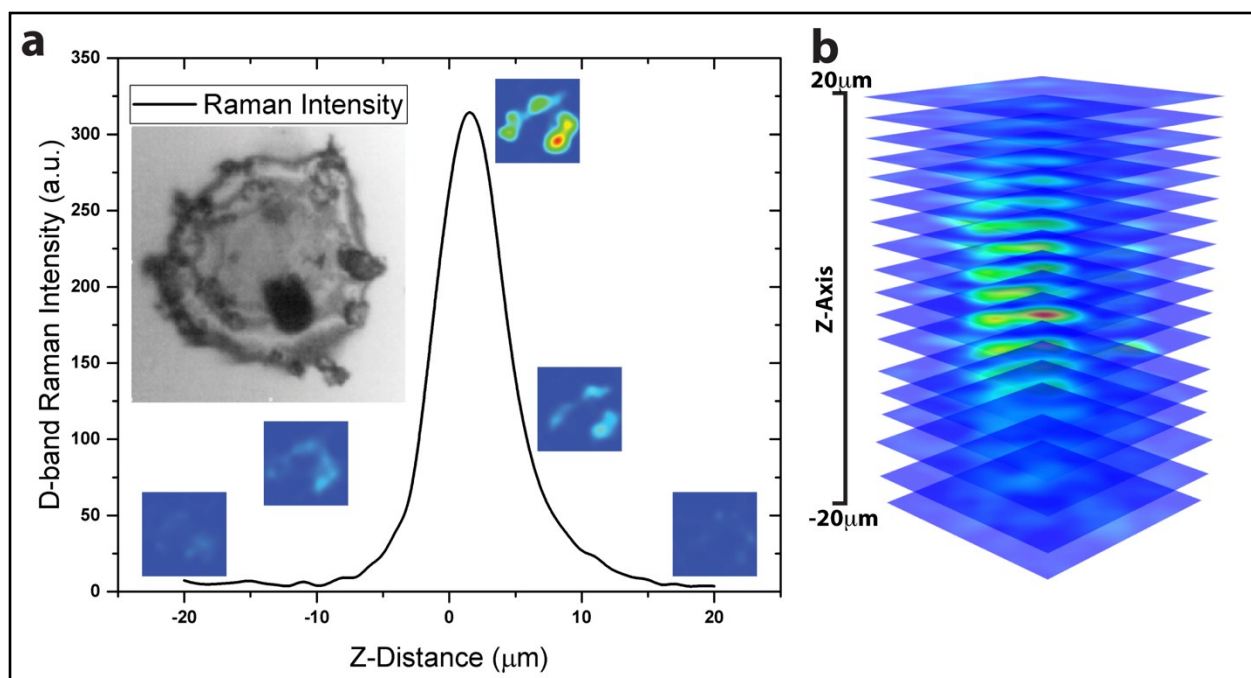


**Figure S13.** z-height mapping of JWASII cell that incubated with 50 $\mu$ g/ml of LOG for 6 hours. (a) D-band intensity as a function of z-distance in ( $\mu$ m) showing that most of the signal comes at around 0-1  $\mu$ m height, (b) Stacking of mapping images of the same cell starting at -20  $\mu$ m and end at 20  $\mu$ m height with 2  $\mu$ m increment between each map.

**Video S3.** 3D view of the mapping slices that showing the graphene signal was coming from both surface and cytoplasm of the representative scanned cell (JWASII). The slices were assembled using ImageJ to produce 3D rotating video.

## Graphene Sedimentation Rate (kinetics of sedimentation)

To assess the stability of graphene dispersion in cell media, the following experiments were conducted.

- 50 and 1  $\mu\text{g}/\text{ml}$  of LOG solutions were prepared in JAWSII media and in PC12 media. then the solution was transferred to UV-Visible spectrophotometer cuvettes and the media (no graphene) was used as a reference solution.
- Sedimentation rate of LOG solutions were studied as a function of time (kinetics). LOG samples in media were scanned from 300 to 800 nm periodically every 30 minutes for 24 hours. The results are presented in figure (S14, S15).

As a result of these experiments, LOG dispersion in media solutions were stable over 24h, for 1  $\mu\text{g}/\text{ml}$  there were no loose in the solution concentration over that period of time, However, 50  $\mu\text{g}/\text{ml}$  loses around 2% of the initial concentration. Results are presented in SI figure S15.

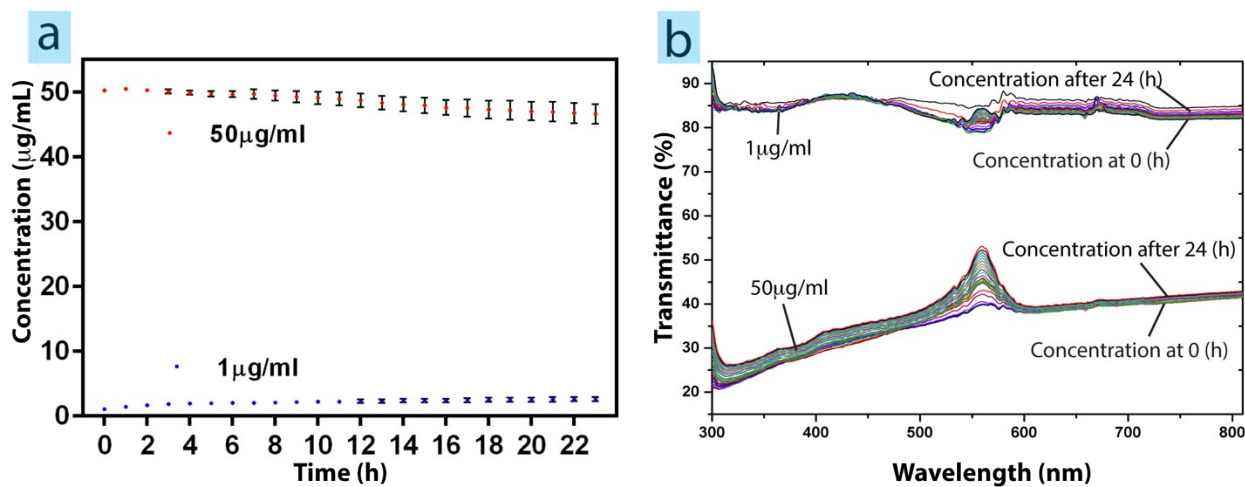


**Figure S14.** LOG sedimentation rate (kinetic of sedimentation rate), (a): 50 and 1  $\mu\text{g}/\text{mL}$  of LOG in JAWSII media within interval of 30 minutes starting from 0 to 24 hours ( $n=3$ ). (b) transmittance spectra for two concentration (1, 50  $\mu\text{g}/\text{mL}$ ) of LOG in JAWSII media, scanned from 300 to 800 nm periodically every 30 minutes for 24 hours.

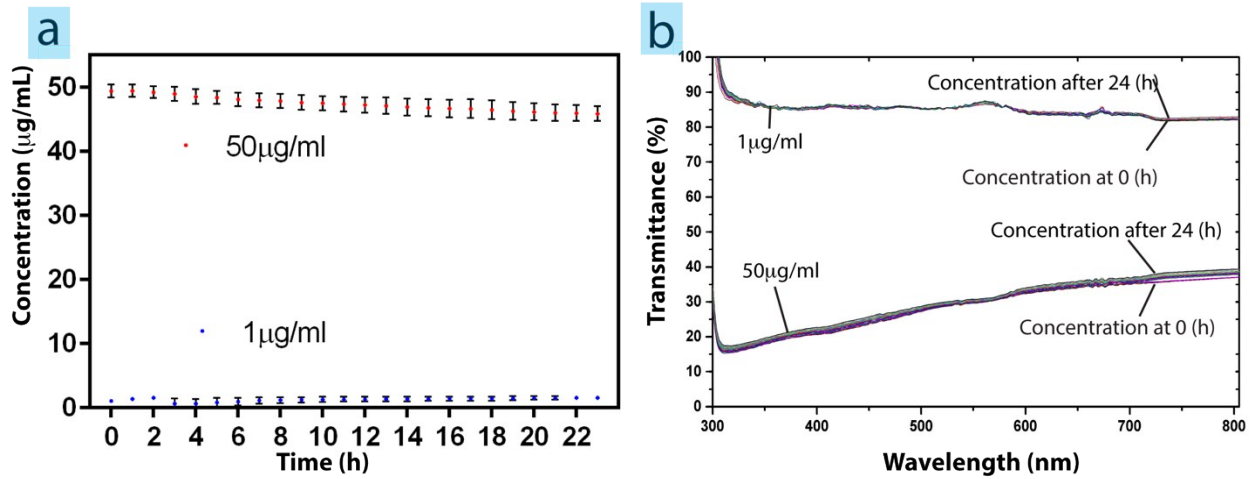


**Figure S15:** LOG sedimentation rate (kinetic of sedimentation rate), (a): 50 and 1  $\mu\text{g/mL}$  of LOG in PC12 media within interval of 30 minutes starting from 0 to 24 hours ( $n=3$ ). (b) transmittance spectra for two concentration (1, 50  $\mu\text{g/mL}$ ) of LOG in PC12 media scanned from 300 to 800 nm periodically every 30 minutes for 24 hours.

### Dynamic Light Scattering (DSL) study

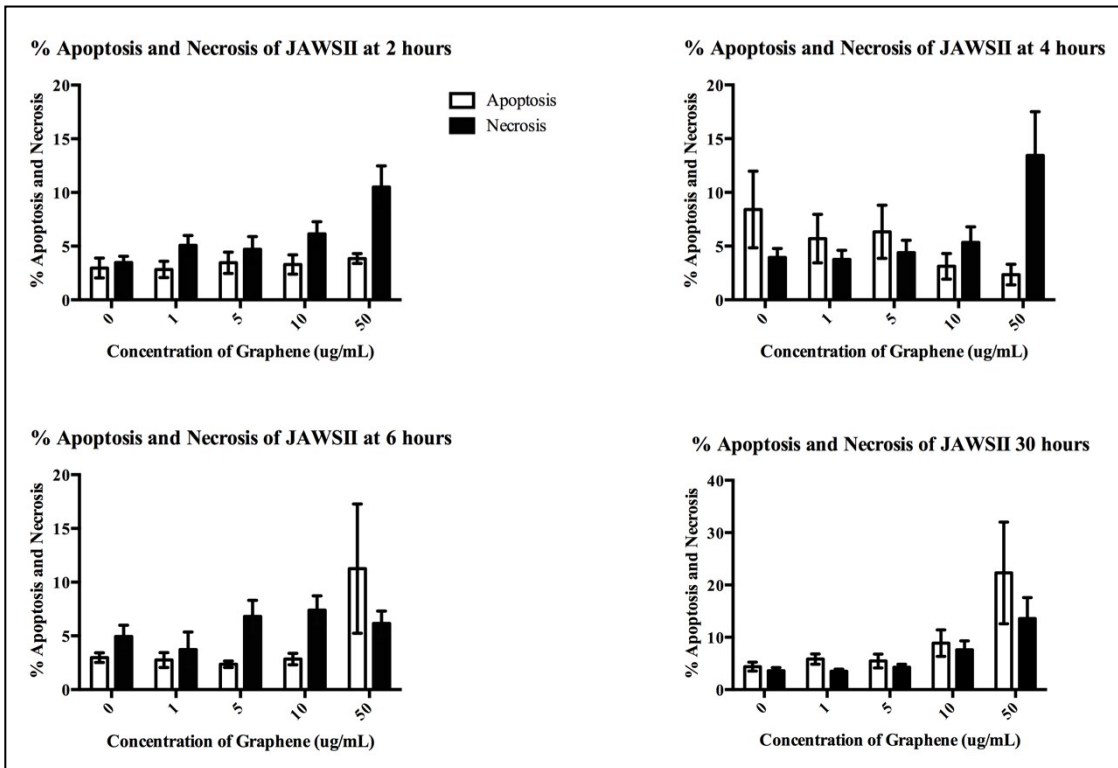
Dynamic Light Scattering: Graphene stock solution was bath sonicated for 30 minutes before we prepared the test concentrations of 1  $\mu\text{g/ml}$  and 5  $\mu\text{g/ml}$  graphene in DI water and cell culture medium (Jaws II and PC12) respectively. Test samples were sonicated again for 5 minutes just before reading the samples. A 200- $\mu\text{l}$  sample was put in a disposable micro cuvette (Malvern, Westborough, MA) to find the dynamic size data using a Zetasizer Nano-Zs (Malvern) with the material specification reference file for graphene. After taking the initial reading at day 0 samples were saved and read again after 24 hours. Data were collected from three independent experiments conducted on different days.

**Table S1.** Estimation of graphene dynamic size using the dynamic light scattering technique.

LOG in Water					
Time	Water Only	PC12 Medium only	JAWSII Medium Only	1 $\mu\text{g/ml}$	5 $\mu\text{g/ml}$
0 Hour	0	33.8 $\pm$ 0.1	39.8 $\pm$ 12.9	328.1 $\pm$ 6.3	313.0 $\pm$ 6.4
24 Hours	0	35.9 $\pm$ 0.5	126.7 $\pm$ 4.5	316.8 $\pm$ 4.5	307.4 $\pm$ 6.2

## Toxicity analysis of JAWSII cells exposed to graphene

Since JAWSII cells were observed to phagocytose/endocytose graphene, the impact of graphene on the induction of cellular apoptosis was assessed using flow cytometry. In cells stained with Annexin V and PI, we determined the doses that induce apoptosis, assessing distinct populations of cells undergoing apoptosis and necrosis: live cells (Annexin V- PI-), early apoptosis (Annexin V+ PI-), late apoptosis, (Annexin V+ PI+) and necrotic cells (Annexin V- PI+) (Fig. S16). For our purposes, we designated the gates Annexin V+ PI- and Annexin V+ PI+ as our general apoptosis gate. Using this as our indicator of total percent apoptosis in JAWSII cells, we observed no statistical difference in % apoptosis when cells were treated with medium alone or with 1, 5, 10, and 50  $\mu\text{g}/\text{mL}$  of graphene for the 2, 4, 6, or 30 h time points (Fig. S16). However, by 30 hours, at the 50  $\mu\text{g}/\text{mL}$  concentration, the % apoptosis had increased to 22%.



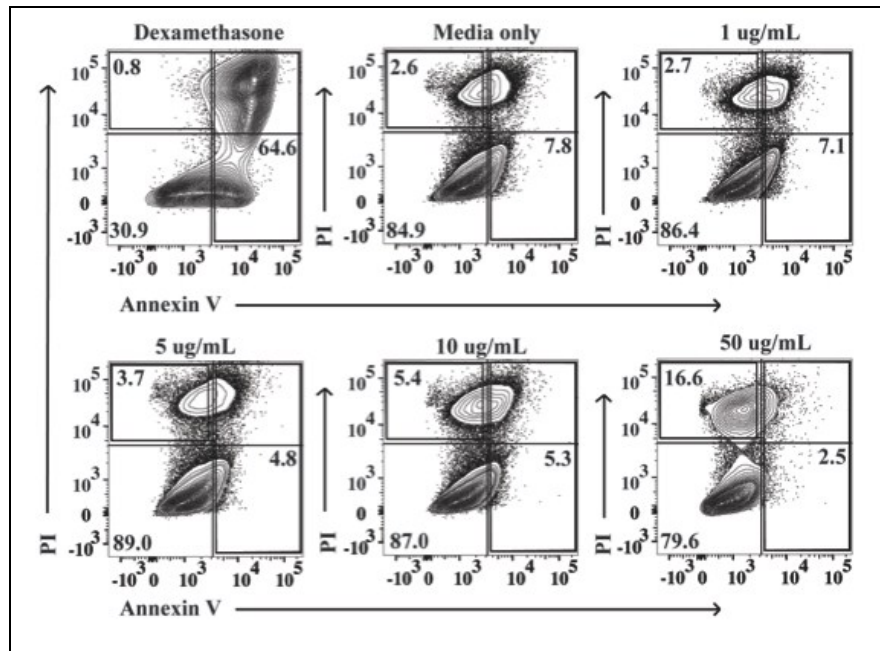


**Figure S16.** Graphene is relatively noncytotoxic. Percent apoptosis in JAWSII cells remains steady. Cells were treated with 1, 5, 10, and 50  $\mu\text{g}/\text{mL}$  of graphene and dexamethasone (+ control) or medium alone for 30 hours and then stained for Annexin V and analyzed by flow cytometry. The combined data are based on three independent experiments and are expressed as mean  $\pm$  standard error of the mean,  $n = 6-8$ . There was no statistical difference in percent apoptosis+ cells of JAWSII cells (open bars) in the given treatment conditions at any time point as performed using the Mann Whitney Test.

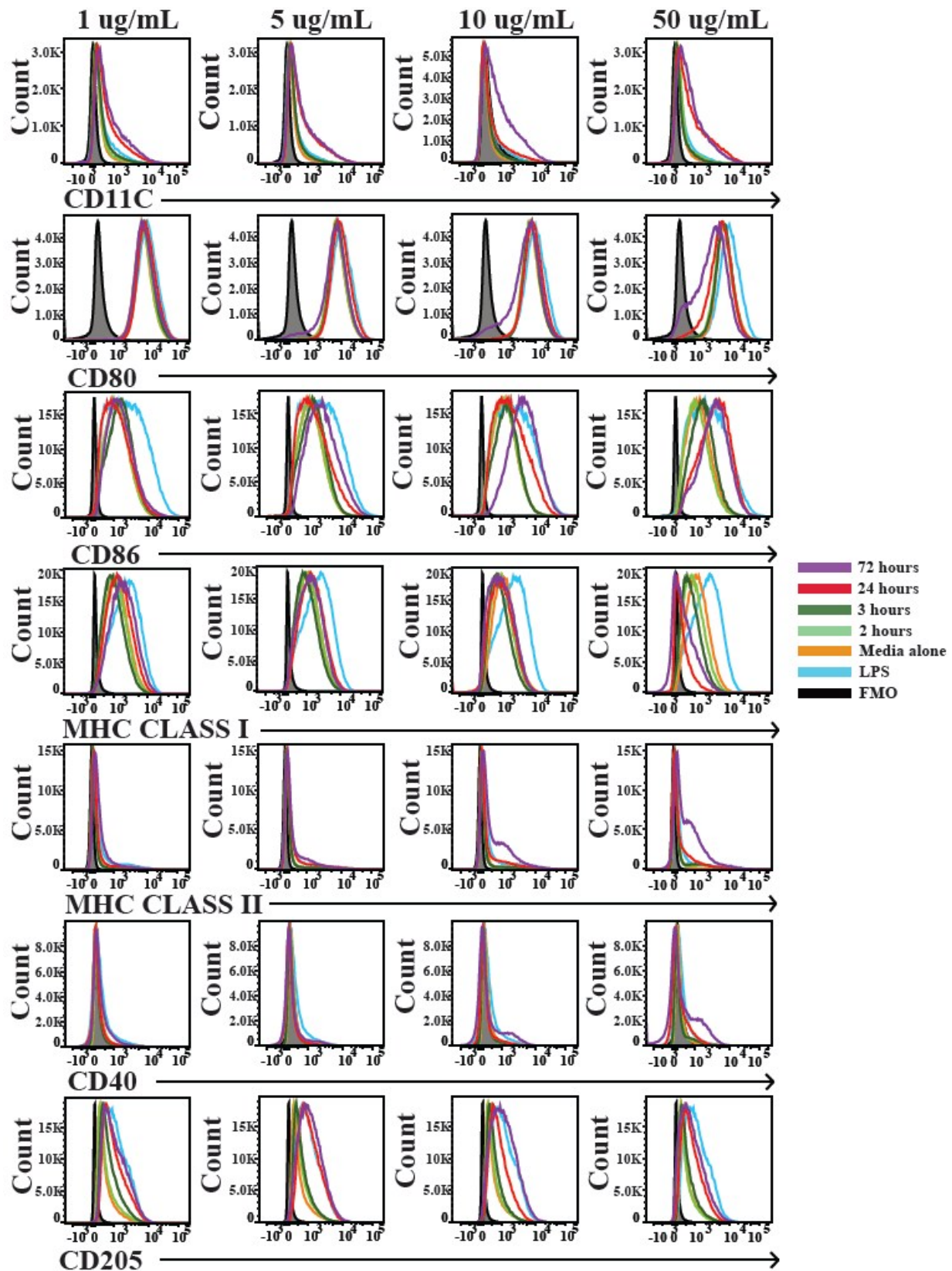
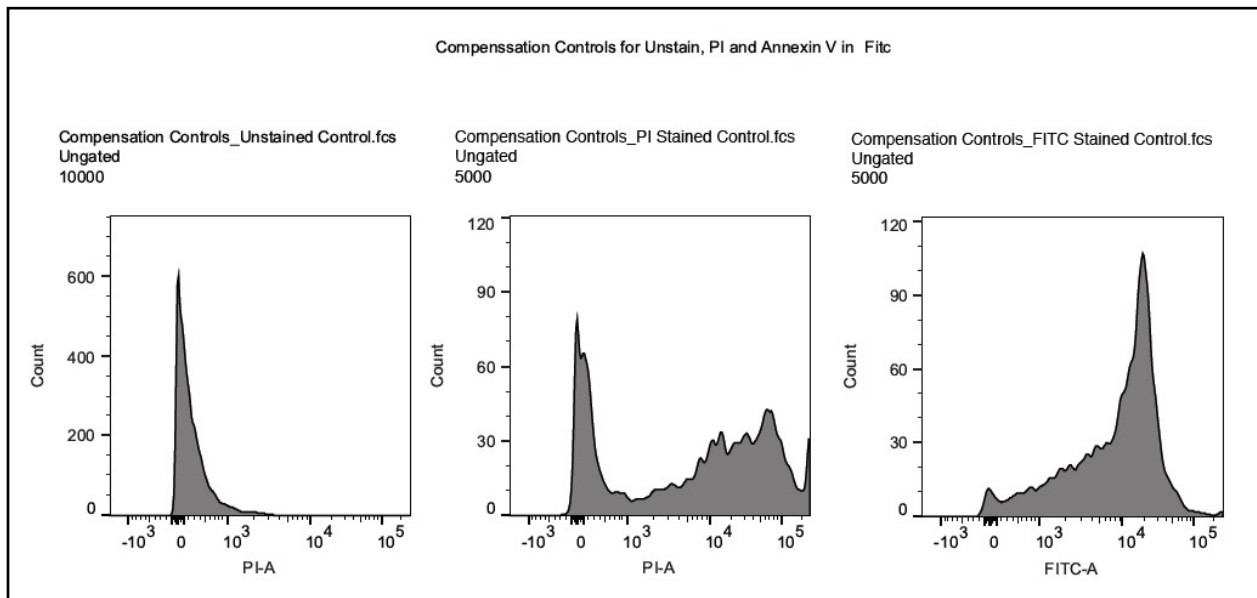


Figure S17. Dynamic surface receptor expression on JAWSII cells after graphene treatment.

JAWSII cells were treated with medium alone (orange histogram), 5  $\mu\text{g/mL}$  LPS (blue histogram), or the following concentrations of graphene: 1  $\mu\text{g/mL}$  (far left), 5  $\mu\text{g/mL}$  (middle left), 10  $\mu\text{g/mL}$  (middle right), and 50  $\mu\text{g/mL}$  (far right) for 2 hours (light green histogram), 3 hours (dark green histogram), 24 hours (red histogram), and 72 hours (purple histogram). Data are representative of two independent experiments; n=2-3 per treatment condition.

### Compensation Control for Unstain, PI, and Annexin V in Fite.



**Figure S18.** Compensation controls for Annexin V/PI experiments. Cells were either untreated or treated with dexamethasone (apoptosis+ control) for 30 hours and then stained for Annexin V and PI and analyzed by flow cytometry. Shown in left panel is the live = unstained controls, middle panel = PI single stain, and right panel = Annexin V apoptosis single stain controls.

## Raman spectra for LOG with 514nm Laser

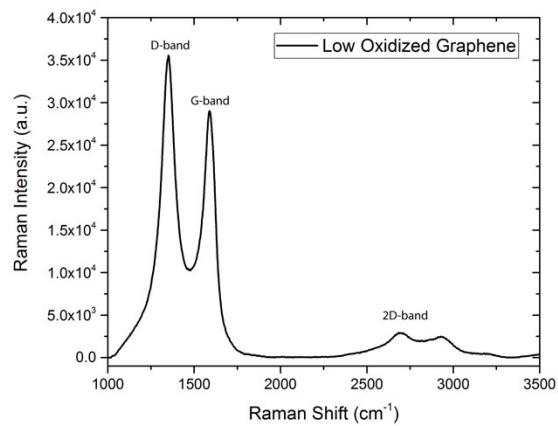


**Figure S19.** Raman spectrum for LOG recorded by using 514nm laser. G and D band intensity ratio was used to calculate the crystalline structure of graphene flakes.

## Statistical Analysis of Raman data

### 1. JAWSII cells

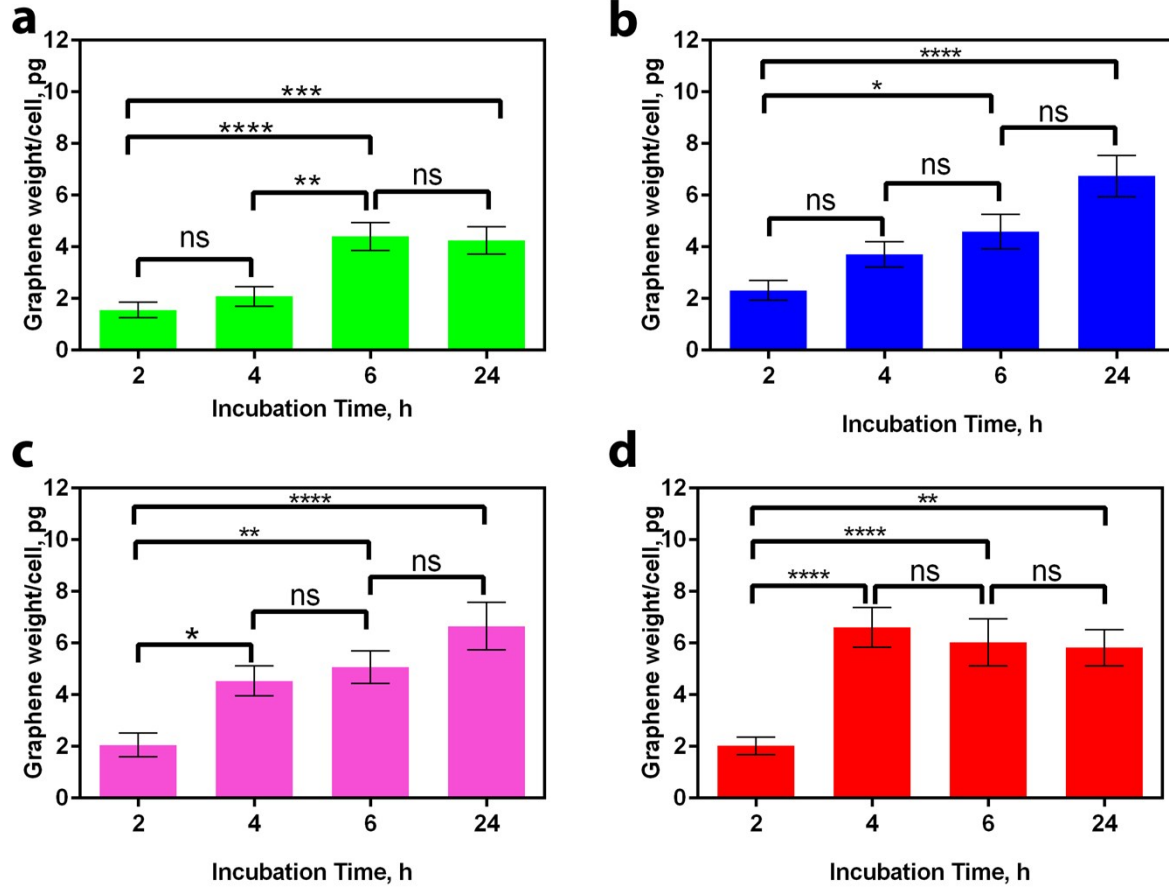


**Figure S20.** Ordinary one-way ANOVA statistical analysis for JAWSII cells incubated with 1, 5, 10, 50 µg/ml, *ns*: non-significant,  $P < 0.05$ , confidence limits  $CL = 95\%$ . a) 1 µg/ml, b) 5 µg/ml, c) 10 µg/ml, and d) 50 µg/ml.

## 2. MDA-231 cells

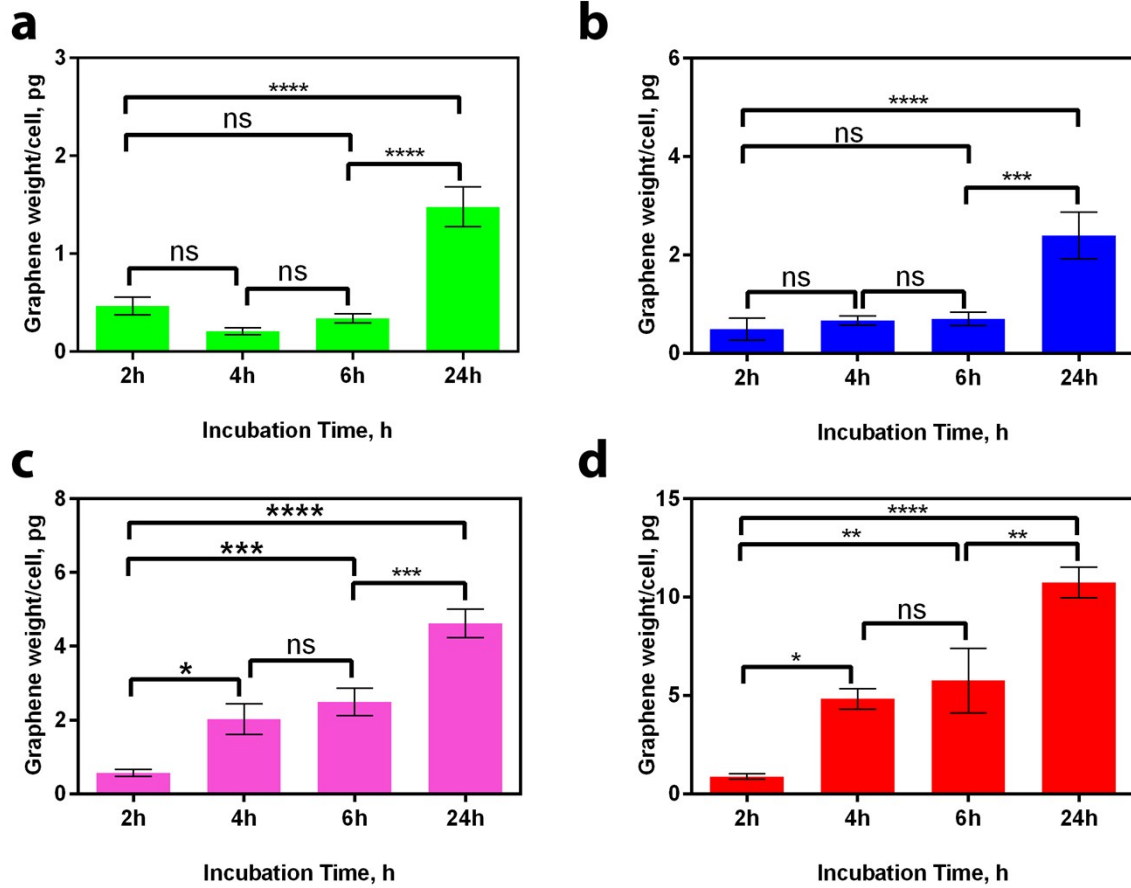


**Figure S21.** Ordinary one-way ANOVA statistical analysis for MDA-231 cells incubated with 1, 5, 10, 50 µg/ml, *ns*: non-significant,  $P < 0.05$ , Confidence limits  $CL = 95\%$ . a) 1 µg/ml, b) 5 µg/ml, c) 10 µg/ml, and d) 50 µg/ml.

### 3. PC12 cells

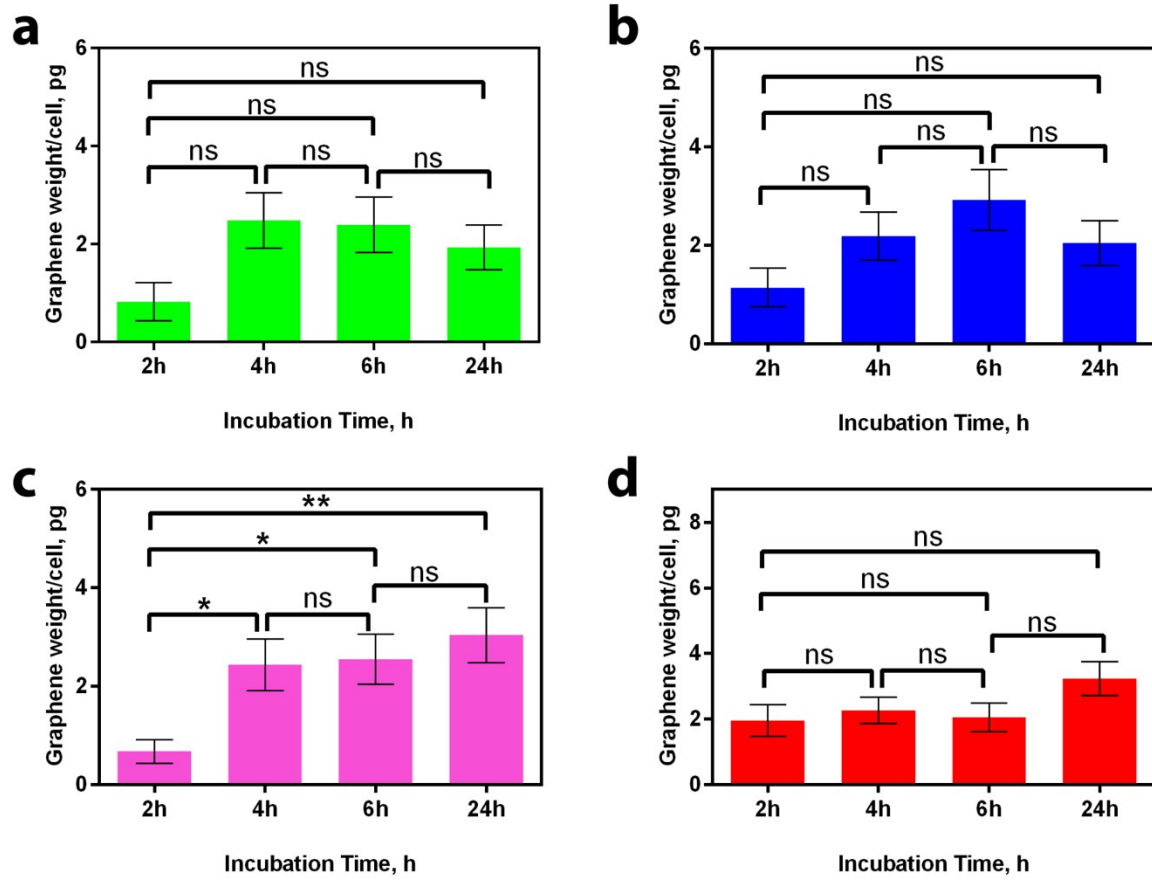


**Figure S22.** Ordinary one-way ANOVA statistical analysis for PC12 cells incubated with 1, 5, 10, 50  $\mu\text{g/ml}$ , *ns*: non-significant,  $P < 0.05$ , Confidence limits  $CL = 95\%$ . a) 1  $\mu\text{g/ml}$ , b) 5  $\mu\text{g/ml}$ , c) 10  $\mu\text{g/ml}$ , and d) 50  $\mu\text{g/ml}$ .

## References

- 1 Yang, D. *et al.* Chemical analysis of graphene oxide films after heat and chemical treatments by X-ray photoelectron and Micro-Raman spectroscopy. *Carbon* **47**, 145-152, doi:<http://dx.doi.org/10.1016/j.carbon.2008.09.045> (2009).
- 2 Datsyuk, V. *et al.* Chemical oxidation of multiwalled carbon nanotubes. *Carbon* **46**, 833-840, doi:<http://dx.doi.org/10.1016/j.carbon.2008.02.012> (2008).
- 3 Wojtoniszak, M. *et al.* Synthesis, dispersion, and cytocompatibility of graphene oxide and reduced graphene oxide. *Colloids and Surfaces B: Biointerfaces* **89**, 79-85, doi:<http://dx.doi.org/10.1016/j.colsurfb.2011.08.026> (2012).
- 4 Robert M. Silverstein, G. Clayton Bassler & Morrill, T. C. *Spectrometric Identification of Organic Compounds*. (Wiley and Sons, 1981).